RSC Advances

ROYAL SOCIETY OF CHEMISTRY

www.rsc.org/advances

RSC Advances

ARTICLE

Visible light photoelectrochemical properties of hydrogenated TiO_2 nanorod film and its application in the detection of chemical oxygen demand

Received 00th January 20xx,
Accepted 00th January 20xx

DOI: 10.1039/x0xx00000x

www.rsc.org/

Xiujie Wang[a], Shengsen Zhang[b, ‡], Hongjuan Wang[a], Hao Yu[a], Haihui Wang[a], Shanqing Zhang[a,c], Feng Peng[a, ‡]

A series of TiO_2 nanorod array electrodes with different lengths have been successfully fabricated by a controlled hydrothermal method for photoelectrochemical (PEC) application. In order to enhance the conductivity of the Ti nanorods and enable the PEC activity under visible light irradiation, the TiO_2 nanorods samples have been further hydrogenated. The influence of the length of hydrogenated TiO_2 nanorod arrays (H-TNRs) on their visible-light-driv photoelectrocatalytic activity was investigated. With increasing the length of the H-TNRs to about 3.0 μm, the activity was close to the maximum. Subsequently, the H-TNRs photoanode was fitted into a thin-layer photoelectrochemical cell for mineralization of organic compounds. The visible light PEC performance was enhanced so much that chemical oxygen demand (COD) detection was achieved under visible light as light source for the first time. Excellent relationship betwee the photoelectrochemical COD and conventional COD values within the range of 0-288 mg L^{-1} suggests that the simple visible light driven PEC method is a promising alternative to the conventional COD method.

1. Introduction

In the last decade, One-dimensional (1D) TiO_2 including nanorods, nanowires, and nanotubes have been extensively investigated since it confirmed to be superior photoelectrochemical (PEC) properties to other dimensional TiO_2 nanostructures.[1-6] Among them, single crystal TiO_2 nanorods (TNRs) or nanowires further offer direct electrical pathways for photogenerated electrons and could increase the oriented charge separation and the electron transport rate,[7-11] and the length of nanorods is a key factor influencing the charge collection efficiency. Yang *et al.* reported that, with increasing the length of the single crystalline rutile TiO_2 nanorods to about 1.8 μm, the photocurrent density was close to the maximum.[12] Bian *et al.* investigated the effects of the length (0.68-2.3 μm) of TiO_2 nanorod on the PEC properties of TiO_2 nanorod/C dot nanocomposites, photocatalytic activity reached a maximum with the length of 1.3 μm.[13] However, the mainly application of single crystalline rutile TNRs was photoelectrochemical water splitting[9, 12, 14-16] and solar cells[7, 8, 17-19]. The application in determination of chemical oxygen demand (COD) was seldom reported.

In recent years, a photoelectrochemical probe for rapid determination of COD is developed using a nanostructured TiO_2 photoanode, namely PeCOD.[20-24] As compared to the standard analytical method, PeCOD method is more promising because of the superior oxidative ability of illuminated TiO_2. Furthermore, TiO_2 nanomaterials are typically non-toxic, inexpensive, photostable, and environmentally benig However, the drawback of TiO_2-based methods in practical applications is the easy recombination of the photogenerated electron/hole pairs in discrete TiO_2 nanoparticles and coated nanofilm, which results in low photocatalytic activity. Different from the TiO_2 coated on transparent conducting oxides (TCO) glass electrode, Zhou's group[24-26] fabricated TiO_2 nanotube arrays (TNTs) on Ti sheet as the COD sensor. The TNTs well suit for the efficient separation of photogenerated holes because the TNTs electrode is highly ordered with high aspect-ratio structures and nanocrystalline walls perpendicular to electrically conductive Ti substrates. Wang et al. investigated the application of TiO_2 nanorod arrays to the determination of COD and well correlated with those obtained using the conventional (i.e., dichromate) COD determination method. Li et al.[27] prepared hydrogenated TNTs (H-TNTs) to improve the conductivity and PEC efficiency, which was also used to detect COD under UV-light irradiation. However, both the TNTs, TNRs and coated-TiO_2 nanoparticles film electrode have an inevitable drawback that is the limiting use of the light sourc for the wide band gap of 3.2 or 3.0 eV.[28] It is necessary to u e the UV light source to excite the photogenerated electron/hole pairs. The instrument user inevitable suffers U V irradiation. Therefore, some catalysts with visible-light-photoactivity as COD sensor have been studied presently. F r

[a] School of Chemistry and Chemical Engineering, South China University of Technology, Guangzhou 510640, China. Email: cefpeng@scut.edu.cn (F. Peng).
[b] College of Materials and Energy, South China Agricultural University, Guangzhou, 510642, China. Email: Shengsenz@126.com (S. Zhang).
[c] Centre for Clean Environment and Energy, Griffith School of Environment, Gold Coast Campus, Griffith University, QLD 4222, Australia.

example, Chao *et al.*[29] used the Cu_2O-loaded TiO_2 nanotube arrays electrode as PeCOD sensor to detect COD using visible light, however, the lifetime of the electrode was not desirable enough as the Cu_2O particles suffer from photocorrosion. WO_3/W nanopores sensor for COD determination under visible light has been reported, but the working range (3-60 mg L^{-1}) is too narrow.[30] In the previous reports, we prepared hydrogenated TiO_2 nanorod arrays (H-TNRs) used as a photoelectrode, which exhibited highly sensitive and steady photocurrent to the investigated organic compounds under visible light,[31] indicating that it could be a promising photoelectrochemical sensor for organic compounds in water solution. However, visible light PEC properties of the H-TNRs film dependence on nanorod lengths and its application in the detection of COD have not been investigated.

Herein, we further investigated the influence of the length of the H-TNRs on their visible-light-driven photoelectrocatalytic activity and designed photoelectrochemical sensor with a thin-layer cell for COD detection. Different from the conventional TiO_2 photocatalytic sensor which needs the irradiation of UV light, the prepared H-TNRs electrode as photoelectrochemical sensor can detect COD value of the real samples using visible light.

2. Experimental

2.1 Preparation of H-TNRs

TNRs with different lengths were prepared on a fluorine-doped tin oxide (FTO) glass slide using our previous work.[31] Briefly, 20.0 mL deionized water was mixed with 20.0 mL of concentrated hydrochloric acid (36.5 wt%) in a Teflon-lined stainless steel autoclave (100 mL). The mixture was stirred at ambient conditions for 5 min before the addition 0.48 mL of titanium butoxide (97% Aldrich). After stirring for another 5 min, two pieces of FTO substrates (5×2 cm^2) were cleaned in a sequence of acetone, absolute alcohol and deionized water and dried in air, and subsequently placed into the Teflon-liner at an angle against the wall with the conducting side facing down. The hydrothermal synthesis was conducted at 170 °C for different time, i.e., 3 h, 6 h, 9 h and 12 h, and denoted as TNRs-3, TNRs-6, TNRs-9, and TNRs-12, respectively. The obtained samples were taken out, rinsed with deionized water, and dried in air. The H-TNRs electrodes were prepared via the hydrogenation process of the TNRs in argon (80 mL min^{-1}) and hydrogen (20 mL min^{-1}) mixed atmosphere at 350 °C in a tubular furnace under ambient pressure for 1 h with a heating rate of 5 °C min^{-1}.

2.2 Characterization of samples

The surface morphologies and cross-sectional structures of the samples were characterized by scanning electron microscope (FESEM, LEO 1530VP). X-ray diffraction (XRD) analysis was carried out with an X-ray diffractometer (D/max-IIIA, Japan), Cu *Kα* radiation (λ=1.5418 Å) and a fixed power source (40 kV and 40 mA) were used. UV-vis diffuse reflectance spectroscopy (DRS) measurement was conducted by a UV-1601 spectrophotometer (Shimazu, Japan). The chemical nature of Ti and O was studied using X-ray photoelectron spectroscopy (XPS) in Krato Axis Ultra DLD spectrometer with Al K*α* X-ray (*hv*=1486.6 eV) at 15 kV and 150 W. The binding energy was referenced to C 1s line at 284.6 eV for calibration.

2.3 Apparatus and measurements

All photoelectrochemical experiments were performed at the room temperature (25 °C) in a thin photoelectrochemical cell with a quartz window for visible light illumination (see Figure 1). It consists of a three-electrode system with an H-TNRs film working electrode, a saturated Ag/AgCl reference electrode and a platinum mesh counter electrodes. The flow path and the photoelectrochemical reaction zone were confined by a shaped spacer with thickness of 0.1 mm. A quartz window (0.5×1 cm^2) was embedded into the front Teflon board and used to admit illumination. All interstices were sealed with silicone gel to keep the reactor airtight. The photocurrent-time curves in this work were measured using an electrochemical workstation (CHI 660B, Shanghai) coupled with a computer. A PLS-SXE300UV Xe lamp was used as the light source and the UV part of the light was removed by a UV-400 filter when the process was carried out. The incident light intensity (100 mW cm^{-2}) was measured by a radiant power meter (400-1000 nm, FZ-A radiation meter, Beijing Normal University).

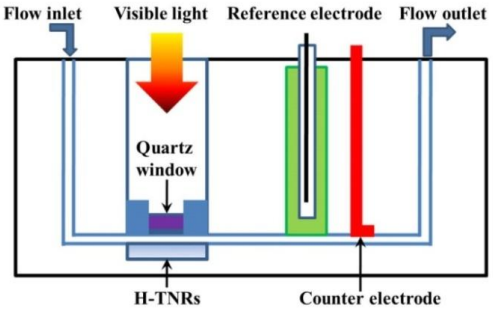

Figure 1. Schematic depiction of the thin-layer cell photoelectrochemical cell for continuous flow analysis.

3. Results and discussion

3.1 Structure characterizations

H-TNRs with different lengths were obtained by controlling the growth time at 170 °C. Figure 2A-D show the top-down and cross section morphologies of H-TNRs-3, H-TNRs-6, H-TNRs-9 and H-TNRs-12, respectively. The corresponding average equivalent diameters of H-TNRs were measured to about 80, 170, 200 and 220 nm and the density of the nanorods decreased by increasing the hydrothermal synthetic time. Figure 2A shows the H-TNRs-3 with the length of 0.6 μm has not obvious vertical array structure, while the nanorods begin to grow on the FTO substrate with the rod axis perpendicular to the substrate. And after 3 h, the top surface of the nanorods appears to contain many step edges, while the side surface is smooth, which is consistent with the work by Aydil et al.[7] Moreover, from H-TNRs-6 to H-TNRs-12, the overall lengths of the nano-layer are about 1.8, 3.0 and 3.8 μm, respectively. However, except the underneath non-array structure layer, the lengths of nanorod arrays are about 1.2, 2.0 and 2.0 μm in H-TNRs-6, H-TNRs-9 and H-TNRs-12, respectively.

ARTICLE

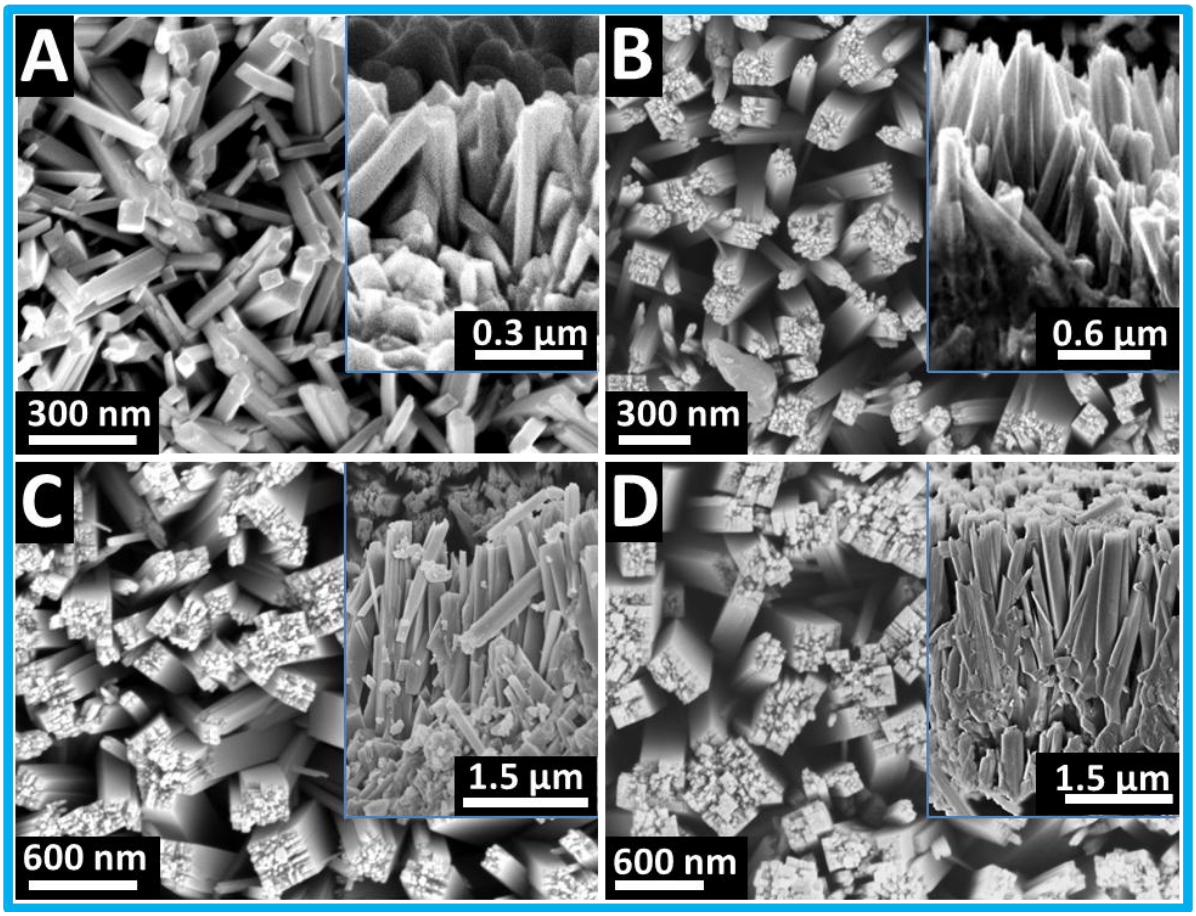

Figure 2. FESEM images of (A) H-TNRs-3, (B) H-TNRs-6, (C) H-TNRs-9 and (D) H-TNRs-12. Insets are corresponding cross-sections.

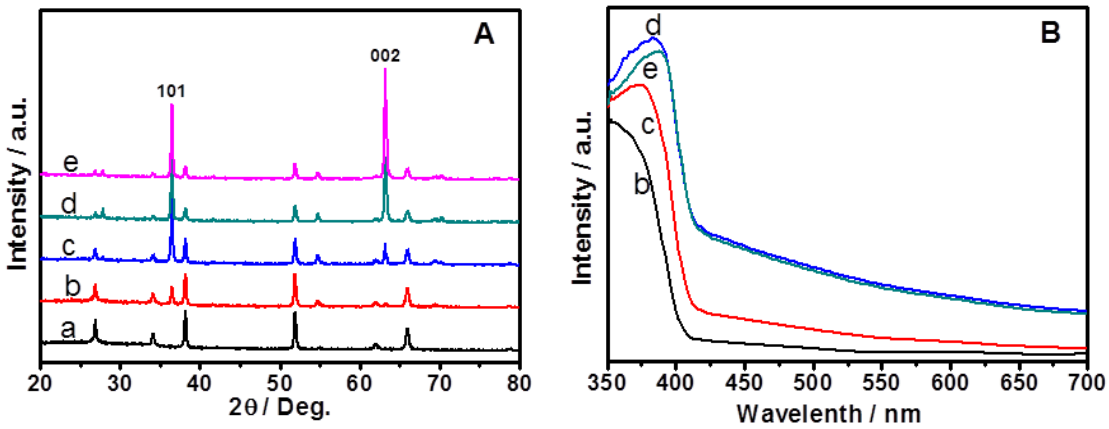

Figure 3. (A) XRD and (B) UV-vis DR spectra of the (a) FTO, (b) H-TNRs-3, (c) H-TNRs-6, (d) H-TNRs-9 and (e) H-TNRs-12.

Figure 3A shows the XRD spectra of the FTO glass and different H-TNRs samples. After subtracting the diffraction peaks of FTO glass, two diffraction peaks centered at 2θ angles of 36.5° and 63.2° were observed in every sample, corresponding to (101) and (002) crystal planes of tetragonal rutile TiO_2, respectively (JCPDS No. 88-1175). The intensity of the (002) peak increases rapidly with the increase of synthetic time, suggesting that the TiO_2 nanorods are highly oriented in the (001) direction with respect to the FTO substrate surface and grow in the (001) direction with the growth axis parallel to the substrate surface normal.[7, 32] Therefore, the length of TiO_2 nanorods increases with the synthetic time, which is consistent with the results from Figure 2. In addition, there is no significant difference among the intensities of the (101) peaks of H-TNRs-6, H-TNRs-9 and H-TNRs-12, indicating that the equivalent diameters of the H-TNRs are similar (170-220 nm). The diffraction peaks of FTO glass decrease with the increase of the synthetic time due to the

increase of the density and length of TiO_2 nanorods on the FTO glass. These results from XRD spectra confirmed that the rutile TiO_2 nanorods were grown directionally on the FTO glass and the hydrothermal synthetic time had an important influence on the TiO_2 growth.

Figure 3B exhibits the UV-visible light absorption of the H-TNRs increases dramatically with the hydrothermal synthetic time from 3 to 9 h due to the more and longer TiO_2 nanorods on FTO. However, the absorption decreases slightly when the synthetic time reaches to 12 h. This can be explained by the observation on Figure 2. Compared with H-TNRs-9, H-TNRs-12 possesses larger TiO_2 nanorods, which lead to the stronger light reflection and the reduction of the light diffusion. Consequently, the H-TNRs-12 has a slightly weaker light absorption than H-TNRs-9.

High-resolution Ti $2p_{3/2}$ and O 1s XPS spectra of the H-TNRs-9 were displayed in Figure 4. The Ti $2p_{3/2}$ XPS spectrum can be separated two peaks at 458.3 and 457.6 eV, which can be ascribed to Ti^{4+} and Ti^{3+}. The result demonstrates the presence of Ti-O and oxygen vacancies in TiO_2, which is in line with the literatures[2, 33] and our previous reports.[27, 31] The O 1s XPS spectrum can be deconvoluted into two peaks centered at 529.9 and 531.8 eV. One at 529.9 eV corresponds to the characteristic peak of Ti-O-Ti.[34] The other at 531.8 eV is attributed to Ti-OH, which has been reported to be located at ca. 1.5-1.8 eV higher binding energy corresponding to the O 1s of unhydrogenated-TiO_2.[32] The result confirmed the formation of hydroxyl group on H-TNRs-9 surface.

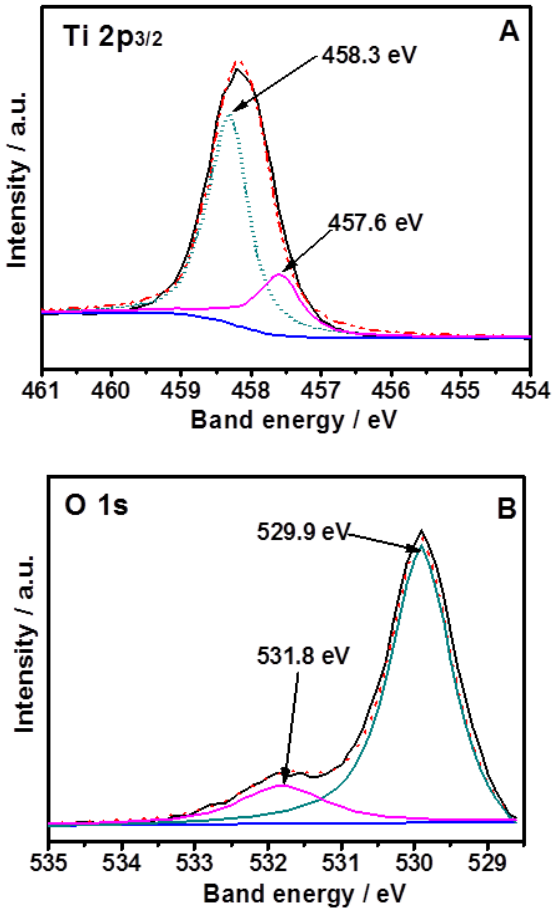

Figure 4. XPS spectra of (A) Ti 2p3/2 and (B) O1s of H-TNRs-9.

3.2 Photoelectrochemical properties and COD detection

The photocurrent density was tested in a thin photoelectrochemical cell. A 0.1 M $NaNO_3$ solution was used as supporting electrolyte. The photocurrent of TNRs without hydrogenation under visible light irradiation is approximately zero, as our reported before.[31] Figure 5A shows that the dark current is approximately zero under a constant applied potential of +0.10 V (vs Ag/AgCl). However, under visible light illumination, the photocurrent spikes and then reaches a relatively steady state after 40 s for all the HTNRs samples, which is related to the following reasons. Hydrogenation of TiO_2 crystal can create oxygen vacancy and Ti^{3+} sites, leading to shallow donor states between the conduction band and valence band, namely mid-gap energy levels. This is responsible for the absorption of longer wavelength of light (>400 nm).[32, 35] Moreover, hydrogen atoms can stay in TiO_2 crystal lattice as shallow donors enhancing the charge transport capability (electronic conductivity), promoting the PEC reaction.[31, 36] The average steady photocurrent density is increasingly enhanced when the length of the H-TNRs changes from 0.6 to 3.0 µm. With the increase in the length of H-TNRs, the more charge carriers are generated by photo-stimulation due to the stronger visible-light absorption. When the overall length of H-TNRs increases from 3.0 µm to 3.8 µm, a decrease in photocurrent density is observed. Although the absorption of light decreases slightly, the photocurrent density decreases obviously. It can be explained that the photogenerated charge carriers in the top part of the H-TNRs-12 should diffuse a longer distance to reach the FTO film, and the recombination probability of the charge carriers during the transport is largely increased, leading to the significantly decreased photocurrent.

Figure 5B shows the photocurrent-time plots of H-TNRs-9 electrode as a sensor to different concentrations of glucose. The photocurrent ($I_{background}$) observed for the blank solution (dash line) originates from the oxidation of water by the illuminated H-TNRs-9, whereas the photocurrent (I_{total}) observed in the organic (glucose) solution is the summation of two components (solid line), one arising from the oxidation of glucose and the other arising from the oxidation of water.[25, 37] The decay of the I_{total} to the $I_{background}$ level implies that all the glucose have been oxidized in the thin-cell reactor. Furthermore, the quantity of net charges (Q_{net}) originating from the photoelectrochemical oxidation of the glucose increases with the increasing concentration of glucose. It is also notable that the I_{total} for the all samples is the almost same value from 150 to 200 s, which means the excellent stability and reproducibility of H-TNRs.

ARTICLE

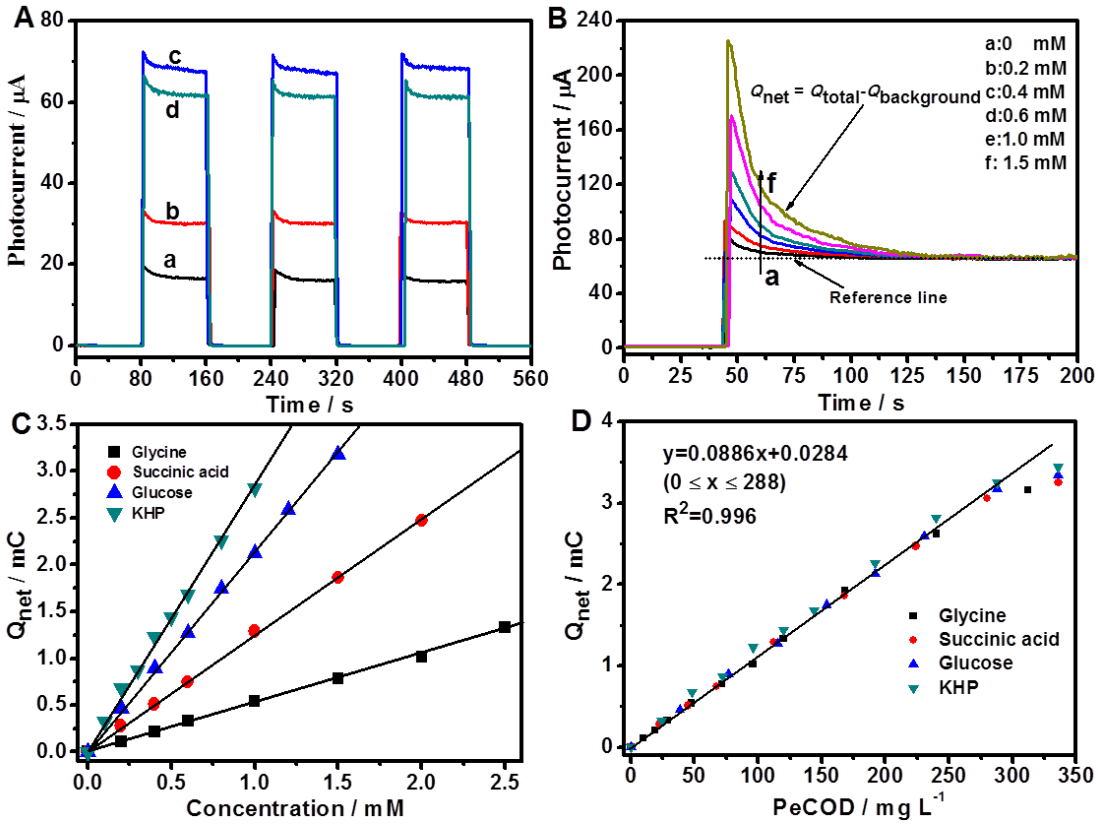

Figure 5. (A) Photocurrent responses of (a) H-TNRs-3, (b) H-TNRs-6, (c) H-TNRs-9 and (d) H-TNRs-12; (B) Photocurrent responses of H-TNRs-9 as a sensor in different concentrations of glucose; (C) Quantitative relationship between Q_{net} and the concentration of organic compounds with H-TNRs-9 as a sensor; (D) Quantitative relationship Q_{net} and the theoretical COD.

Other three organic compounds (glycine, succinic acid and potassium hydrogen phthalate (KHP)) solutions were investigated and exhibited similar voltammograms to those shown in Figure 5B (not shown here). The Q_{net} can be calculated according to Faraday's law, and the quantitative relationship between Q_{net} and the concentration of organic compounds have been established, as shown in Figure 5C. It can be seen that for all organic compounds investigated, the quantity of net charges obtained are directly proportional to the concentration.

Since one oxygen molecule corresponds to the transfer of four electrons (Eq.(1)), the measured Q_{net} value can be converted to an equivalent O_2 concentration (or oxygen demand). The equivalent COD value can then be represented as Eq.(2).[38]

$$O_2 + 4H^+ + 4e^- \longrightarrow 2H_2O \quad (1)$$

$$\text{COD (mg L}^{-1}\text{ of O}_2) = \frac{nC}{4} \times 32000 = \frac{Q_{net}}{4FV} \times 32000 = KQ_{net} \quad (2)$$

Figure 5D has been derived from Figure 5C by plotting the Q_{net} against theoretical COD values according to Eq. (2). The plot reveals that all the compounds investigated here can be fitted by straight line y = 0.0886x + 0.0284 with a R^2 value of 0.996 in the range of 0-288 mg L^{-1}. The excellent linear relationship between Q_{net} and the theoretical COD suggests that the H-TNRs electrode can be adopted as visible-light-driven PeCOD sensor for various organic compounds.

Figure 6 displays the correlation between the PeCOD method and standard dichromate method for COD measurement of the real samples, including two lake water, four civic sewage, four garbage leakage, and two dyeing wastewater. The trend line has a slope of 1.000 with correlation coefficient (R^2) of 0.985. A comparison of two methods shows a highly significant correlation for both PeCOD and COD measurements, indicating that the simple and rapid PeCOD method using visible light as light sources is a reliable alternative to the conventional dichromate method.

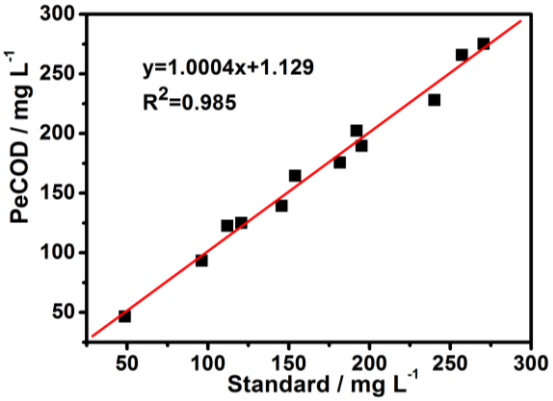

Figure 6. The correlation between the PeCOD method and conventional dichromate method for the real sample measurements.

Conclusions

In this work, the influence of the length of the hydrogenated TiO_2 nanorod arrays on their visible-light-driven photoelectrocatalytic activity has been investigated. The optimal sample, i.e., H-TNRs-9, has been used as a photoelectrochemical sensor for COD detection using visible light as light source for the first time, and provided a relative wide dynamic working rang of 0-288 mg L^{-1}. The results showed a good relationship between photoelectrochemical COD and practical COD values for the real samples. Moreover, the H-TNRs photoanode exhibited good stability and reproducibility. These advantages suggest that the hydrogenated TiO_2 nanorods would be a promising and practical photoanode as a new photoelectrochemical sensor for online COD monitoring using the visible light as the excitation light.

Acknowledgments

We acknowledge the financial support from the National Natural Science Foundation of China (No. 21328301), the Guangdong Provincial Natural Science Foundation (No. 2014A030312007) and the Fundamental Research Funds for the Central Universities (No. 2014ZM0052).

Notes and references

1 H. Liu, G. Xu, J. Wang, J. Lv, Z. Zheng and Y. Wu, *Electrochim. Acta*, 2014, **130**, 213-221.
2 C. Zhang, H. Yu, Y. Li, Y. Gao, Y. Zhao, W. Song, Z. Shao and B. Yi, *ChemSusChem*, 2013, **6**, 659-666.
3 K. Shankar, J.I. Basham, N.K. Allam, O.K. Varghese, G.K. Mor, X.J. Feng, M. Paulose, J. A. Seabold, K.S. Choi and C.A. Grimes, *J. Phys. Chem. C*, 2009, **113**, 6327-6359.
4 J. Chen, Z. Xia, H. Li, Q. Li and Y. Zhang, *Electrochim. Acta*, 2015, **166**, 174-182.
5 J.Y. Liao, B.X. Lei, H.Y. Chen, D.B. Kuang and C.Y. Su, *Energy Environ. Sci.*, 2012, **5**, 5750-5757.
6 J.I. Kim, J.M. Park, S.J. Hwang, M.J. Kang and J.C. Pyun, *Anal. Chim. Acta*, 2014, **836**, 53-60.
7 B. Liu and E. S. Aydil, *J. Am. Chem. Soc.*, 2009, **131**, 3985-3990.
8 W. Yang, Y. Wang and W. Shi, *CrystEngComm*, 2012, **14**, 230-234.
9 Y. Yang, G. Wang, Q. Deng, S. Kang, D.H.L. Ng and H. Zhao, *CrystEngComm*, 2014, **16**, 3091-3096.
10 X. Feng, K. Shankar, O.K. Varghese, M. Paulose, T.J. Latempa and C.A. Grimes, *Nano Lett.*, 2008, **8**, 3781-3786.
11 H.S. Kim, D.T. Nguyen, E.C. Shin, J.S. Lee, S.K. Lee, K.S. Ahn and S.H. Kang, *Electrochim. Acta*, 2013, **114**, 159-164.
12 Y.J. Hwang, C. Hahn, B. Liu and P. Yang, *ACS nano*, 2012, **6**, 5060-5069.
13 J. Bian, C. Huang, L. Wang, T. Hung, W.A. Daoud and R. Zhang, *ACS Appl. Mater. Interfaces*, 2014, **6**, 4883-4890.
14 C. Wang, Z. Chen, H. Jin, C. Cao, J. Li and Z. Mi, *J. Mater. Chem. A*, 2014, **2**, 17820-17827.
15 H. Wang, Y. Bai, H. Zhang, Z. Zhang, J. Li and L. Guo, *J. Phys. Chem. C*, 2010, **114**, 16451-16455.
16 F. Su, T. Wang, R. Lv, J. Zhang, P. Zhang, J. Lu and J. Gong, *Nanoscale*, 2013, **5**, 9001-9009.
17 G. Dai, L. Zhao, J. Li, L. Wan, F. Hu, Z. Xu, B. Dong, H. Lu, S. Wang and J. Yu, *J. Colloid Interface Sci.*, 2012, **365**, 46-52.
18 Z.J. Zhou, J.Q. Fan, X. Wang, W.Z. Sun, W.H. Zhou, Z.L. Du and S.X. Wu, *ACS Appl. Mater. Interfaces*, 2011, **3**, 2189-2194.
19 M. Li, Y. Liu, H. Wang, H. Shen, W. Zhao, H. Huang and C. Liang, *J. Appl. Phys.*, 2010, **108**, 094304.
20 S. Zhang, D. Jiang and H. Zhao, *Environ. Sci. Technol.*, 2006, **40**, 2363-2368.
21 J. Bai and B. Zhou, *Chem. Rev.*, 2014, **114**, 10131-10176.
22 C. Wang, J. Wu, P. Wang, Y. Ao, J. Hou and J. Qian, *Anal. Chim. Acta*, 2013, **767**, 141-147.
23 X. Li, W. Yin, J. Li, J. Bai, K. Huang, J. Li and B. Zhou, *Water Environ. Res.*, 2014, **86**, 532-539.
24 S. Yuan, R. Mao, Y. Li, Q. Zhang and H. Wang, *Electrochim. Acta*, 2012, **60**, 347-353.
25 Q. Zheng, B. Zhou, J. Bai, L. Li, Z. Jin, J. Zhang, J. Li, Y. Liu, W. Cai and X. Zhu, *Adv. Mater.*, 2008, **20**, 1044-1049.
26 J. Zhang, B. Zhou, Q. Zheng, J. Li, J. Bai, Y. Liu and W. Cai, *Water Res.*, 2009, **43**, 1986-1992.
27 S. Li, J. Qiu, M. Ling, F. Peng, B. Wood and S. Zhang, *ACS Appl. Mater. Interfaces*, 2013, **5**, 11129-11135.
28 A. Bendavid, P.J. Martin, A. Jamting and H. Takikawa, *Th Solid Films*, 1999, **355**, 6-11.
29 C. Wang, J. Wu, P. Wang, Y. Ao, J. Hou and J. Qian, *Sen Actuators B*, 2013, **181**, 1-8.
30 X. Li, J. Bai, Q. Liu, J. Li and B. Zhou, *Sensors*, 2014, **14**, 1068 10690.
31 S. Zhang, S. Zhang, B. Peng, H. Wang, H. Yu, H. Wang and F. Peng, *Electrochem. Commun.*, 2014, **40**, 24-27.
32 G. Wang, H. Wang, Y. Ling, Y. Tang, X. Yang, R. C. Fitzmorris, C. Wang, J. Z. Zhang and Y. Li, *Nano Lett.*, 2011, **11**, 3026 3033.
33 Y. Yan, M. Han, A. Konkin, T. Koppe, D. Wang, T. Andreu, G. Chen, U. Vetter, J. R. Morante and P. Schaaf, *J. Mater. Chem. A*, 2014, **2**, 12708-12716.
34 X. Chen, L. Liu, P. Y. Yu and S. S. Mao, *Science*, 2011, **331**, 746-750.
35 A. Naldoni, M. Allieta, S. Santangelo, M. Marelli, F. Fabbri, S. Cappelli, C. L. Bianchi, R. Psaro and V. Dal Santo, *J. Am. Chem Soc.*, 2012, **134**, 7600-7603.
36 W. D. Zhu, C. W. Wang, J. B. Chen, D. S. Li, F. Zhou and H. L. Zhang, *Nanotechnology*, 2012, **23**, 455204.
37 H. Zhao, D. Jiang, S. Zhang, K. Catterall and R. John, *Anal. Chem.*, 2004, **76**, 155-160.
38 S. Zhang, H. Zhao, D. Jiang and R. John, Anal. Chim. Acta, 2004, **514**, 89-97.